

Jamming of Deformable Polygons

Arman Boromand,^{1,2} Alexandra Signoriello,³ Fangfu Ye,^{1,4} Corey S. O'Hern,^{2,3,5,6} and Mark D. Shattuck⁷

¹Beijing National Laboratory for Condensed Matter Physics and CAS Key Laboratory of Soft Matter Physics, Institute of Physics, Chinese Academy of Sciences, Beijing, China

²Department of Mechanical Engineering and Materials Science, Yale University, New Haven, Connecticut 06520, USA

³Program in Computational Biology and Bioinformatics, Yale University, New Haven, Connecticut 06520, USA

⁴School of Physical Sciences, University of Chinese Academy of Sciences, Beijing, China

⁵Department of Physics, Yale University, New Haven, Connecticut 06520, USA

⁶Department of Applied Physics, Yale University, New Haven, Connecticut 06520, USA

⁷Benjamin Levich Institute and Physics Department, The City College of the City University of New York, New York, New York 10031, USA

 (Received 18 January 2018; revised manuscript received 13 May 2018; published 11 December 2018)

We introduce the deformable particle (DP) model for cells, foams, emulsions, and other soft particulate materials, which adds to the benefits and eliminates deficiencies of existing models. The DP model combines the ability to model individual soft particles with the shape-energy function of the vertex model, and adds arbitrary particle deformations. We focus on 2D deformable polygons with a shape-energy function that is minimized for area a_0 and perimeter p_0 and repulsive interparticle forces. We study the onset of jamming versus particle asphericity, $\mathcal{A} = p_0^2/4\pi a_0$, and find that the packing fraction grows with \mathcal{A} until reaching $\mathcal{A}^* = 1.16$ of the underlying Voronoi cells at confluence. We find that DP packings above and below \mathcal{A}^* are solidlike, which helps explain the solid-to-fluid transition at \mathcal{A}^* in the vertex model as a transition from tension- to compression-dominated regimes.

DOI: 10.1103/PhysRevLett.121.248003

There are many physical systems that can be modeled as packings of soft, *deformable* particles, including cell monolayers [1–3], developing tissues [4–6], compressed foams [7], and emulsions [8]. We introduce the deformable particle (DP) model, which has advantages over previous models used to describe these systems. The DP model considers deformable particles described by an energy function that depends on particle shape, allows motion of individual particles, can include different particle interactions over a range of packing fractions ϕ , and is easily defined in two (2D) and three (3D) spatial dimensions.

The key feature of the DP model is that the particle shape is described by many degrees of freedom (d.o.f.). The shape and position of the particles evolve under Newton's equations of motion according to a shape-energy function, inter-particle forces, and external forces. Models based only on particle centers, such as the soft disk model [9,10], are not deformable in this sense. Even if the particle perimeter and area can change, as in Voronoi-based models [11–13], the particle shape in these models is completely determined by the particle center, although they can include complex multiparticle interactions. In the vertex model [14,15], each vertex is shared by at least 3 cells, which also constrains particle shapes. In addition, the vertex and Voronoi-based models are limited to confluent systems, $\phi = 1$. An extension of the vertex model to nonconfluent systems has been developed [13], but it uses Voronoi

tessellation with a finite-size cutoff to determine particle shape, and the particle boundary is not described by independent d.o.f.

Soft disk models allow studies of the onset of jamming of 2D soft particulate materials as a function of ϕ , whereas the vertex model allows studies of the onset of jamming as a function of particle shape, e.g., the asphericity, $\mathcal{A} = p^2/4\pi a$, where p and a are the particle perimeter and area [16]. The DP model enables studies of jamming as a function of *both* ϕ and \mathcal{A} . We focus on 2D and model N deformable “particles” (indexed by $m = 1, \dots, N$) as polygons with N_v vertices (indexed by $i = 1, \dots, N_v$) to represent $N_v - 1$ shape d.o.f. The location of the i th vertex in polygon m is $\vec{v}_{m,i}$, the bond vector $\vec{l}_{m,i} = \vec{v}_{m,i+1} - \vec{v}_{m,i} = l_{m,i}\hat{l}_{m,i}$ connects vertices $i + 1$ and i , and $p_m = \sum_{i=1}^{N_v} l_{m,i}$. A general 2D shape-energy function that can describe soft, particulate systems is

$$\begin{aligned}
 U = & \frac{k_l N_v}{2} \sum_{m=1}^N \sum_{i=1}^{N_v} (l_{m,i} - l_0)^2 + \frac{k_a}{2} \sum_{m=1}^N (a_m - a_0)^2 \\
 & + \gamma \sum_{m=1}^N \sum_{i=1}^{N_v} l_{m,i} + \frac{k_b}{2N_v} \sum_{m=1}^N \sum_{i=1}^{N_v} \left(\frac{2(\hat{l}_{m,i} - \hat{l}_{m,i+1})}{l_{m,i} + l_{m,i+1}} \right)^2 \\
 & + U_{\text{int}}. \tag{1}
 \end{aligned}$$

Equation (1) includes five terms: (1) a contractility term, where adjacent vertices are connected via linear springs, with

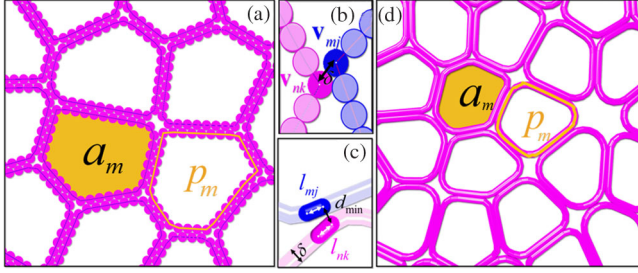


FIG. 1. Schematic of deformable polygons with $N_v = 34$ vertices (with the position of the j th vertex in the m th polygon given by $\vec{v}_{m,j}$), area a_m , and perimeter p_m . $l_{m,j} = p_m/N_v$ is the line segment between vertices j and $j+1$ in polygon m . Two methods were used to model edges of deformable polygons. In (a) and (b), we show the RS method, which fixes centers of disks with diameter δ at polygon vertices. In (c) and (d), we show the SS method, which models polygon edges as circulo-lines with width δ . d_{\min} is the minimum distance between line segments $l_{m,j}$ and $l_{n,k}$.

spring constant per vertex k_l and equilibrium length l_0 , (2) a compressibility term, which is quadratic in a_m with a minimum at a_0 , (3) a line tension term proportional to $\gamma l_{m,i}$, (4) a bending energy term with bending rigidity k_b , and (5) a repulsive interaction energy, U_{int} , which prevents overlaps between polygons. The prime on the sum in the last term indicates that it is cyclic, so that \vec{l}_{m,N_v} connects vertex $i = N_v$ and 1. The factors of N_v and N_v^{-1} in the first and fourth terms ensure that Eq. (1) is independent of N_v in the large- N_v limit.

By tuning the parameters in Eq. (1), it can be used to model a variety of soft, particulate systems. (See Supplemental Material [17].) For example, if we set $k_l = k_b = 0$, $\gamma > 0$, and $k_a > 0$, Eq. (1) can model bubbles and emulsions [18]. We can model soft, solid particles by setting $\gamma = 0$, $k_l > 0$, $k_a > 0$, and $k_b > 0$. In this Letter, we focus on the shape-energy function with $k_l > 0$, $k_a > 0$, and $\gamma = k_b = 0$, which has been used to model cell monolayers [14]:

$$U = \frac{k_l N_v}{2} \sum_{m=1}^N \sum_{i=1}^{N_v} (l_{m,i} - l_0)^2 + \frac{k_a}{2} \sum_{m=1}^N (a_m - a_0)^2 + U_{\text{int}}. \quad (2)$$

By nondimensionalizing Eq. (2), one can define the shape parameter, $\mathcal{A} = (N_v l_0)^2 / 4\pi a_0$. For a rigid (regular) polygon with N_v vertices, $\mathcal{A}_v = N_v \tan(\pi/N_v) / \pi$, which reduces to $\mathcal{A}_v = 1$ when $N_v \rightarrow \infty$.

We implement two methods for calculating the repulsive interactions. For the rough surface method (RS), we fix disks with diameter $\delta = l_0 = 1$ at each polygon vertex [Figs. 1(a) and 1(b)]. Repulsive interactions are obtained by summing up repulsive linear spring interactions between overlapping disks on contacting polygons:

$$U_{\text{int}} = \sum_{m=1}^N \sum_{n>m}^N \sum_{j=1}^{N_v} \sum_{k=1}^{N_v} \frac{k_r}{2} (\delta - |\vec{v}_{m,j} - \vec{v}_{n,k}|)^2 \times \Theta(\delta - |\vec{v}_{m,j} - \vec{v}_{n,k}|), \quad (3)$$

where k_r gives the strength of the repulsive interactions, $\vec{v}_{m,j}$ is the position of the j th vertex in polygon m and $\Theta(\cdot)$ is the Heaviside step function. We also implemented a smooth surface method (SS) by modeling polygon edges as circulo-lines with width δ [16] [Figs. 1(c) and 1(d)]. We use Eq. (3) for the repulsive interactions between polygons, except the overlap $(\delta - |\vec{v}_{m,j} - \vec{v}_{n,k}|)$ is replaced by $\delta - d_{\min}$, where d_{\min} is the minimum distance between line segments $l_{m,j}$ and $l_{n,k}$ on contacting polygons m and n .

The DP model includes two geometrical parameters: \mathcal{A} and the diameter of the vertices δ/l_0 for the RS method (or the width of the circulo-lines for the SS method). We seek to characterize geometric properties of DP packings at jamming onset, and thus we focus on the limit $\delta/N_v l_0 \rightarrow 0$. The geometric properties of DP packings at jamming onset do not depend on the two dimensionless energy parameters from Eqs. (2) and (3), $K_1 = k_l/k_a l_0^2$ and $K_2 = k_r/k_l$. Without loss of generality, we set $K_1 = K_2 = 1$ below.

We study DP packings containing $N = 64$ to 10^3 deformable polygons. To generate mechanically stable (MS) packings, we perform isotropic compression with each small increment, $d\phi < 10^{-4}$, followed by molecular dynamics with overdamped dynamics [19]. (See Supplemental Material [17].)

We show the packing fraction at jamming onset ϕ_J (normalized by the maximum packing fraction for each surface roughness model, ϕ_{max}) versus asphericity $\mathcal{A}/\mathcal{A}_v$ for $N = 64$ DP packings in Fig. 2(a). Note that $\phi_{\text{max}} \approx 0.99$ and 0.95 for the smooth and rough surface methods, respectively, for $N_v = 12$ and ϕ_{max} for both methods converges to 1 as $N_v \rightarrow \infty$ [Fig. 2(b)]. $\phi_J/\phi_{\text{max}} \approx 0.82$ – 0.83 (0.88) for the rough (smooth) surface method near $\mathcal{A}/\mathcal{A}_v = 1$ and ϕ_J grows with increasing $\mathcal{A}/\mathcal{A}_v$. The results obtained near $\mathcal{A}/\mathcal{A}_v = 1$ are similar to previous results for jammed packings of monodisperse, frictionless ($\phi_J \approx 0.88$ – 0.89 [20]) and frictional disks ($\phi_J \approx 0.8$ [21]). For $\mathcal{A}/\mathcal{A}_v > 1.02$, ϕ_J/ϕ_{max} has similar dependence on $\mathcal{A}/\mathcal{A}_v$ for the two surface roughness methods. We find similar results for packings of bidisperse deformable polygons (half large with $N_v^l = 17$ and half small with $N_v^s = 12$ and perimeter ratio $r = 1.4$). In Fig. 2(a), we show that $\phi_J(\mathcal{A})$ is similar for $N = 64$ and 10^3 , emphasizing that the system-size dependence is weak. As shown in Fig. 2(b), the packings become confluent with $\phi_J \approx 1$ for $\mathcal{A} > \mathcal{A}^* \approx 1.16$ in the large- N_v limit (since the plateau value of $1 - \phi_J$ decreases with N_v for each model). We note that the self-propelled Voronoi model [12] gives a transition from a disordered solidlike state for $\mathcal{A} < \mathcal{A}_c$ to a liquidlike state for $\mathcal{A} > \mathcal{A}_c$ in the limit of zero particle activity [22], and $\mathcal{A}_c \approx \mathcal{A}^*$.

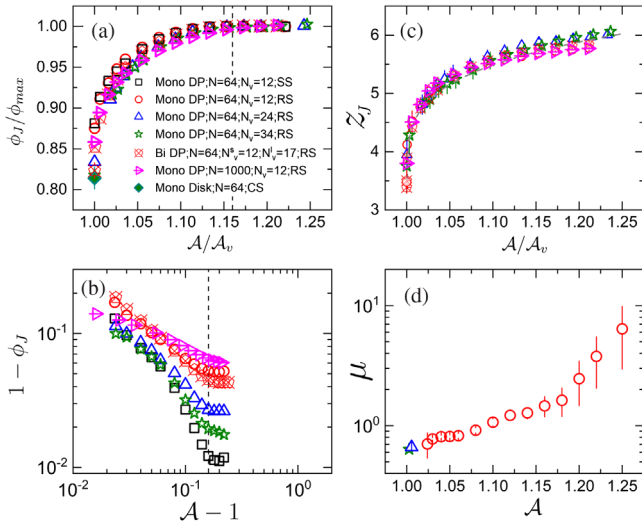


FIG. 2. (a) Packing fraction at jamming onset ϕ_J (normalized by ϕ_{\max}), (b) deviation of ϕ_J from the confluent value, $1 - \phi_J$, (c) coordination number z_J , and (d) average friction coefficient μ (for the RS model) for DP packings versus asphericity \mathcal{A} . In (a) and (c), \mathcal{A} is normalized by \mathcal{A}_v of a regular polygon with N_v vertices. The dashed lines in (a) and (b) indicate $\mathcal{A} = \mathcal{A}^* \approx 1.16$. In (a), we also show $\phi_J/\phi_{\max} \approx 0.81$ (with $\phi_{\max} = 1$) for $N = 64$ monodisperse, frictional discs using the Cundall-Strack (CS) model with $\mu = 0.65$ (filled diamond). In (c), the dashed line indicates $z_J(\mathcal{A}/\mathcal{A}_v) = z_J(1) + z_0(\mathcal{A}/\mathcal{A}_v - 1)^\beta$, where $z_J(1) \approx 3.3$, $\mu = 0.65$, $z_0 \approx 3.9$, and $\beta \approx 0.25$.

In Fig. 2(c), we show the coordination number at jamming onset z_J versus $\mathcal{A}/\mathcal{A}_v$ for deformable polygons for the RS model. Near $\mathcal{A}/\mathcal{A}_v = 1$, $z_J < 4$, which is consistent with studies of packings of frictional disks [23–26]. In contrast, we have shown before that the SS model yields packings with $z_J \approx 4$ near $\mathcal{A}/\mathcal{A}_v = 1$ [16] (when rattler polygons with fewer than 2 interparticle contacts are not included). This result is consistent with isostatic packings [27] of frictionless, monodisperse, and

bidisperse disks. For both roughness models, $z_J(\mathcal{A}/\mathcal{A}_v) - z_J(1)$ increases as a power law in $\mathcal{A}/\mathcal{A}_v - 1$. We find that $z_J = 5.8 \pm 0.1$ at confluence when $\mathcal{A} = \mathcal{A}^*$. In contrast, prior work has suggested that $z_J = 5$ is the isostatic contact number for the vertex model [11].

We also measured the effective friction coefficient $\mu_c = |\vec{F}_{mn}^t|/|\mathbf{F}_{mn}^r|$ at each contact c between polygons m and n in DP packings using the RS model. $|\vec{F}_{mn}^r|$ ($|\vec{F}_{mn}^t|$) is the normal (tangential) component of the repulsive contact force. For each packing, we find the maximum μ_c over all contacts, averaged over at least 500 packings. From previous studies [26], we know that the effective friction coefficient for the RS model scales as $\mu \sim \sqrt{a_0}/N_v \delta$, for $\mathcal{A} \approx 1$. Thus, we can study DP packings with fixed friction coefficient and $\mathcal{A} \rightarrow 1$ by having increases in N_v offset by corresponding increases in $\sqrt{a_0}$. In the large- N_v limit and for $\delta = l_0 = 1$, μ reaches a plateau value, $\mu \approx 0.65$ [Fig. 2(d)]. The contact numbers at jamming onset for $\mu \approx 0.65$ and $\mathcal{A} \rightarrow 1$, $z_J(1) \approx 3.3$ [25,26] (bidisperse) and larger for monodisperse packings [21], are consistent with previous studies. For fixed $N_v = 12$, we show that μ increases by an order of magnitude as \mathcal{A} increases from ≈ 1 to 1.25. We find similar increases for $\mu(\mathcal{A})$ using larger N_v . Despite the strong increase in μ for the RS model, both smooth and rough models yield similar results for $\phi_J(\mathcal{A})$ and $z_J(\mathcal{A})$ away from the rigid-disk limit. Thus, particle deformation weakens the influence of surface friction on the structural properties of DP packings. Note that the RS model can mimic static friction in packings of nonspherical particles for all \mathcal{A} . (See Supplemental Material [17].)

To understand the value $\mathcal{A}^* \approx 1.16$ above which DP packings are confluent, we calculate the free area versus \mathcal{A} using surface-Voronoi tessellation [28–30]. Figure 3 shows example packings at three \mathcal{A} approaching \mathcal{A}^* . At $\mathcal{A} = 1.03$, well below \mathcal{A}^* , the deformable polygons are quasicircular with a relatively large amount of free area. As \mathcal{A} increases, the “effective” sides of the deformable polygons

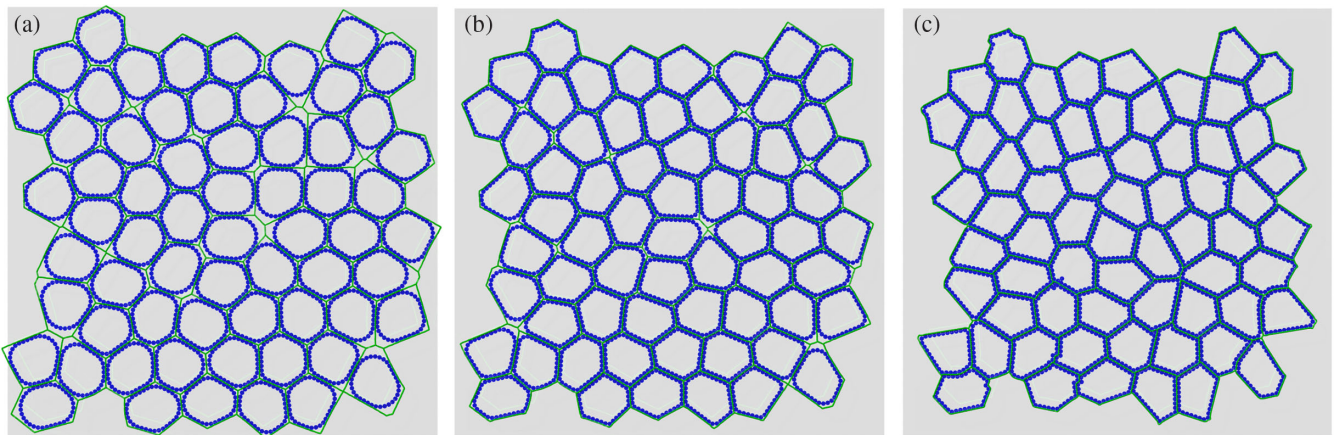


FIG. 3. DP packings for the RS model with $N_v = 34$ and (a) $\mathcal{A} = 1.03$, (b) 1.08, and (c) 1.16, near \mathcal{A}^* . Polygonal cells (solid lines) surrounding each deformable particle are obtained from surface-Voronoi tessellation.

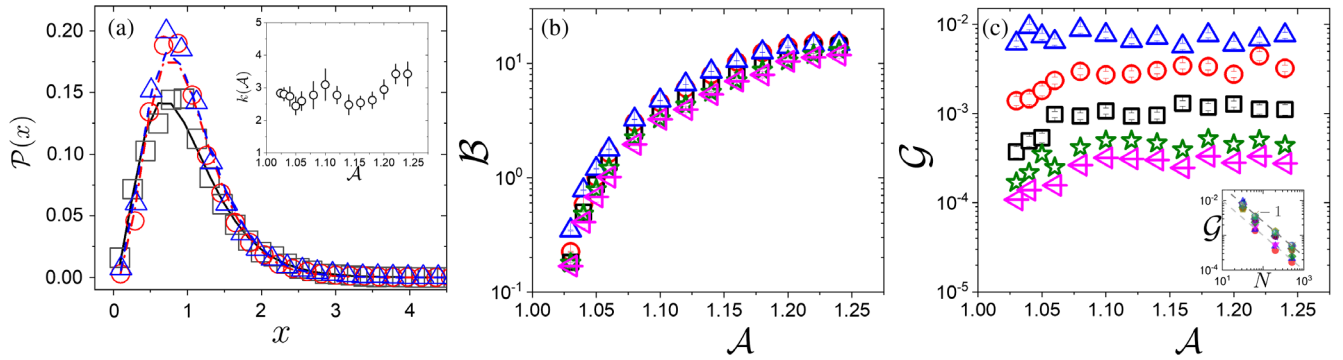


FIG. 4. (a) Distribution of areas a_i of surface-Voronoi tessellated polygons for $\mathcal{A} = 1.03$ (squares), 1.12 (circles), and 1.22 (triangles) for $N = 1000$ monodisperse deformable particles with $N_v = 12$ and the RS model. The distributions $\mathcal{P}(x)$ are plotted against $x = (a_i - a_{\min}) / (\langle a_i \rangle - a_{\min})$, where a_{\min} is the minimum tessellated area for each packing. Fits to the k -gamma distribution [Eq. (4)] are shown as solid, dot-dashed, and dashed lines for $\mathcal{A} = 1.03$, 1.12, and 1.22, respectively. Inset: shape parameter k versus \mathcal{A} from fits of $\mathcal{P}(x)$ to Eq. (4). (b) Bulk \mathcal{B} and (c) shear \mathcal{G} moduli for DP packings using the model in (a) versus \mathcal{A} for $N = 32$ (upward triangles), 64 (circles), 200 (squares), 512 (stars), and 1000 (leftward triangles). The inset to (c) shows system-size scaling of \mathcal{G} . The dashed lines have slope -1 .

straighten and fill the surface-Voronoi cells. When $\mathcal{A} \sim \mathcal{A}^*$, it is difficult to distinguish the deformable polygons from the surface-Voronoi cells. (See Supplemental Material [17].)

Prior studies showed that the areas of Voronoi polygons for hard disks follow k -gamma distributions [31,32]:

$$\mathcal{P}(x) = \frac{k^k}{(k-1)!} x^{k-1} \exp(-kx), \quad (4)$$

where $x = (a_i - a_{\min}) / (\langle a_i \rangle - a_{\min})$, a_i is the area of each Voronoi polygon, a_{\min} is the area of the smallest Voronoi polygon, $\langle a_i \rangle$ is an average over Voronoi polygons, $k = (\langle a_i \rangle - a_{\min})^2 / \sigma_a^2$, and $\sigma_a^2 = \langle (a_i - a_{\min})^2 \rangle$ controls the width of the distribution. In Fig. 4(a), we show that the distribution $\mathcal{P}(x)$ for DP packings resembles a k -gamma distribution with k values that depend on \mathcal{A} . The inset shows k increases from 2.5 to 3.5 over the range $1 < \mathcal{A} < 1.25$. Prior studies reported k values for Voronoi-tessellated hard disks [31] ($k = 3.6$) and jammed bidisperse foams [7] ($k \approx 6$).

Figures 4(b) and 4(c) depict the bulk \mathcal{B} and shear \mathcal{G} moduli for DP packings (RS model with $N_v = 12$) versus \mathcal{A} for several N . (See Supplemental Material [17] for details of the calculations.) \mathcal{B} is roughly independent of N and changes by more than 2 orders of magnitude with \mathcal{A} . In contrast, at each N , \mathcal{G} increases only by a factor of 3 as \mathcal{A} increases from 1 to 1.25. As a result, \mathcal{B}/\mathcal{G} varies from 10^3 to 10^5 , indicating that the system is in the isotropic elastic limit, over this range of \mathcal{A} [33]. The inset of Fig. 4(c) shows that even though DP packings at jamming onset are solidlike with $\mathcal{G} > 0$ for any finite N , \mathcal{G} scales as N^{-1} for all \mathcal{A} . Similar system-size scaling was found for \mathcal{G} in packings of frictionless [34] and frictional [35] disks. The system-size dependence of \mathcal{G} is related to the fact that contacts begin forming and breaking at successively

smaller pressures as N increases. MS packings can be stabilized with $\mathcal{G} > 0$ in the large-system limit by compressing them above ϕ_J . In the Supplemental Material [17], we show that U/N at confluence drops significantly as $\mathcal{A} \rightarrow \mathcal{A}^*$, which is similar to the behavior observed in the vertex model [11].

Other than being confluent for $\mathcal{A} > \mathcal{A}^*$, what is different about DP packings above versus below \mathcal{A}^* ? In the Supplemental Material [17], we show that the excess perimeter $\xi = p - p_{\text{conv}}$ for DP packings, where p_{conv} is the perimeter of the convex hull of each polygon [36]. $p \approx p_{\text{conv}}$ (with $\xi = 0$) for $\mathcal{A} < \mathcal{A}^*$. ξ becomes nonzero for $\mathcal{A} > \mathcal{A}^*$ when deformable polygons buckle and develop invaginations. Thus, DP packings at confluence are under tension for $\mathcal{A} < \mathcal{A}^*$ and under compression for $\mathcal{A} > \mathcal{A}^*$.

In summary, we developed the DP model, which can be used to study packings of 2D deformable particles, including foams, emulsions, and cell monolayers, over a range of packing fraction, particle shape, and deformability. We focused on the DP model for cell monolayers with nonzero k_l and k_a and showed that ϕ_J grows with \mathcal{A} , reaching confluence at $\mathcal{A}^* \approx 1.16$. \mathcal{A}^* coincides with the asphericity at which deformable polygons fill the cells from surface-Voronoi tessellation of DP packings. By calculating their shear modulus \mathcal{G} , we show that DP packings are solidlike above and below \mathcal{A}^* . For $\mathcal{A} > \mathcal{A}^*$, deformable polygons possess invaginations that grow with $\mathcal{A} - \mathcal{A}^*$. Thus, at confluence, DP packings are under compression for $\mathcal{A} > \mathcal{A}^*$ and under tension for $\mathcal{A} < \mathcal{A}^*$.

We acknowledge support from NSF Grants No. PHY-1522467 (A. B.), No. CMMI-1462439 (C. O.), and No. CMMI-1463455 (M. S.), the President's International Fellowship Initiative (PIFI) and Hundred Talents Program of the Chinese Academy of Sciences (A. B. and F. Y.), and the National Library of Medicine

Training Grant No. T15LM00705628 (A. S.). This work was also supported by the High Performance Computing facilities operated by Yale's Center for Research Computing.

-
- [1] M. Sadati, N. T. Qazvini, R. Krishnan, C. Y. Park, and J. J. Fredberg, *Differentiation (Berlin)* **86**, 121 (2013).
- [2] K. E. Kasza, A. C. Rowat, J. Liu, T. E. Angelini, C. P. Brangwynne, G. H. Koenderink, and D. A. Weitz, *Curr. Opin. Cell Biol.* **19**, 101 (2007).
- [3] T. E. Angelini, E. Hannezo, X. Trepate, M. Marquez, J. J. Fredberg, and D. A. Weitz, *Proc. Natl. Acad. Sci. U.S.A.* **108**, 4714 (2011).
- [4] P. Martin and S. M. Parkhurst, *Development* **131**, 3021 (2004).
- [5] F. Serwane, A. Mongera, P. Rowghanian, D. A. Kealhofer, A. A. Lucio, Z. M. Hockenbery, and O. Campàs, *Nat. Methods* **14**, 181 (2017).
- [6] E. Herremans, P. Verboven, B. E. Verlinden, D. Cantre, M. Abera, M. Wevers, and B. M. Nicolai, *BMC Plant Biol.* **15**, 264 (2015).
- [7] G. Katgert and M. van Hecke, *Eur. Phys. Lett.* **92**, 34002 (2010).
- [8] J. Brujić, S. F. Edwards, I. Hopkinson, and H. A. Makse, *Physica (Amsterdam)* **327A**, 201 (2003).
- [9] D. J. Durian, *Phys. Rev. Lett.* **75**, 4780 (1995).
- [10] C. S. O'Hern, L. E. Silbert, A. J. Liu, and S. R. Nagel, *Phys. Rev. E* **68**, 011306 (2003).
- [11] D. Bi, J. H. Lopez, J. M. Schwarz, and M. L. Manning, *Nat. Phys.* **11**, 1074 (2015).
- [12] D. Bi, X. Yang, M. C. Marchetti, and M. L. Manning, *Phys. Rev. X* **6**, 021011 (2016).
- [13] F. Graner and Y. Sawada, *J. Theor. Biol.* **164**, 477 (1993).
- [14] T. Nagai and H. Honda, *Philos. Mag. B* **81**, 699 (2001).
- [15] R. Farhadifar, J.-C. Röper, B. Aigouy, S. Eaton, and F. Jülicher, *Curr. Biol.* **17**, 2095 (2007).
- [16] K. VanderWerf, W. Jin, M. D. Shattuck, and C. S. O'Hern, *Phys. Rev. E* **97**, 012909 (2018).
- [17] See Supplemental Material at <http://link.aps.org/supplemental/10.1103/PhysRevLett.121.248003> for specific details.
- [18] K. A. Brakke, *Exp. Math.* **1**, 141 (1992).
- [19] G.-J. Gao, J. Bławdziewicz, and C. S. O'Hern, *Phys. Rev. E* **74**, 061304 (2006).
- [20] A. Donev, S. Torquato, F. H. Stillinger, and R. Connelly, *J. Appl. Phys.* **95**, 989 (2004).
- [21] L. Kondic, A. Goulet, C. S. O'Hern, M. Kramar, K. Mischaikow, and R. P. Behringer, *Eur. Phys. Lett.* **97**, 54001 (2012).
- [22] Another shape parameter $q = p/\sqrt{a}$, where p and a are the perimeter and area of the particle, is also frequently defined in the literature [12]. The two definitions are related via $A = q^2/4\pi$.
- [23] S. F. Edwards and D. V. Grinev, *Phys. Rev. Lett.* **82**, 5397 (1999).
- [24] R. C. Ball and R. Blumenfeld, *Phys. Rev. Lett.* **88**, 115505 (2002).
- [25] L. E. Silbert, *Soft Matter* **6**, 2918 (2010).
- [26] S. Papanikolaou, C. S. O'Hern, and M. D. Shattuck, *Phys. Rev. Lett.* **110**, 198002 (2013).
- [27] A. V. Tkachenko and T. A. Witten, *Phys. Rev. E* **60**, 687 (1999).
- [28] S. V. Anishchik and N. N. Medvedev, *Phys. Rev. Lett.* **75**, 4314 (1995).
- [29] P. Richard, L. Oger, J. Troadec, and A. Gervois, *Eur. Phys. J. E* **6**, 295 (2001).
- [30] F. M. Schaller, S. C. Kapfer, M. E. Evans, M. J. Hoffmann, T. Aste, M. Saadatfar, K. Mecke, G. W. Delaney, and G. E. Schröder-Turk, *Philos. Mag.* **93**, 3993 (2013).
- [31] V. Senthil Kumar and V. Kumaran, *J. Chem. Phys.* **123**, 114501 (2005).
- [32] T. Aste and T. Di Matteo, *Phys. Rev. E* **77**, 021309 (2008).
- [33] G. N. Greaves, A. Greer, R. Lakes, and T. Rouxel, *Nat. Mater.* **10**, 823 (2011).
- [34] C. P. Goodrich, S. Dagois-Bohy, B. P. Tighe, M. van Hecke, A. J. Liu, and S. R. Nagel, *Phys. Rev. E* **90**, 022138 (2014).
- [35] S. V. Franklin and M. D. Shattuck, *Handbook of Granular Materials, Chapter 6 Packings: Static* (CRC Press, Boca Raton, FL, 2016).
- [36] E. Liu, K. Cashman, and A. Rust, *GeoResJ* **8**, 14 (2015).